Glass Formation, Phase Equilibria, and Thermodynamic Assessment of the Al-Ce-Co System Assisted by First-Principles Energy Calculations

MICHAEL C. GAO, NECIP ÜNLÜ, MAREK MIHALKOVIC, MICHAEL WIDOM, and G.J. SHIFLET

This study investigates glass formation, phase equilibria, and thermodynamic descriptions of the Al-rich Al-Ce-Co ternary system using a novel approach that combines critical experiments, CALPHAD modeling, and first-principles (FP) calculations. The glass formation range (GFR) and a partial 500 °C isotherm are determined using a range of experimental techniques including melt spinning, transmission electron microscopy (TEM), electron probe microanalysis (EPMA), X-ray diffraction, and differential thermal analysis (DTA). Three stable ternary phases are confirmed, namely, Al_8CeCo_2, Al_4CeCo, and $AlCeCo$, while a metastable phase, Al_5CeCo_2, was discovered. The equilibrium and metastable phases identified by the present and earlier reported experiments, together with many hypothetical ternary compounds, are further studied by FP calculations. Based on new experimental data and FP calculations, the thermodynamics of the Al-rich Al-Co-Ce system is optimized using the CALPHAD method. Application to glass formation is discussed in light of present studies.

I. INTRODUCTION

BECAUSE of their promising applications where materials with high specific strength (ratio of fracture strength over density) are desirable, efforts to synthesize bulk Al-rich amorphous alloys have been made for more than a decade. Flexible (the word "flexible" is used because the as-spun amorphous ribbon did not break after a bending test of 180 deg at room temperature) Al-rich Al-TM-RE (TM = transition metals, and RE = rare earth elements) glass-forming systems were discovered at the University of Virginia[1] and elsewhere[2] independently in 1988. Mechanisms for metallic glass formation and prediction of new glass compositions are ongoing areas of intensive research. Empirical rules based upon common features of experimentally identified glass forming systems suggest selecting elements with significant size differences and negative heats of mixing among the major constituents.[3] The discovery of a large body of bulk metallic glasses (BMG) has recently made quantitative analysis of the atomic size distribution in the BMG systems possible. This led to the concept of efficient packing proposed in References 4

and 5. Both the empirical rules and the efficient packing concept help to find favorable combinations of constituent elements. However, what really matters is the critical cooling rate[6,7] that is required to suppress crystallization of each equilibrium and metastable crystalline phase during solidification. The critical cooling rate is commonly and properly used to gage the glass forming ability of a particular alloy. It is often found that only a critical cooling rate of less than ~10 °C/s can lead to formation of BMG.

To quantify the critical cooling rate for each glass forming system, a thermodynamic description is required for at least the equilibrium phases pertaining to metallic glass formation, and a quantitative understanding of atomic diffusion mechanisms is also necessary.[8,9] Although the heat capacity for an amorphous solid can be measured with experiments,[10] metallic glasses often readily crystallize with increasing temperature, and care must be taken to examine whether the sample remains fully amorphous during heat capacity measurement. On the other hand, the thermodynamic descriptions for the equilibrium phases for the system can be obtained by the CALPHAD (calculations of phase diagrams) method, once sufficient data on the phase diagram and thermochemistry are available.

Further, despite their high fracture strength, metallic glasses are rarely used as structural materials due to their shearing instability leading to shear bands resulting in catastrophic failure. Therefore, metallic glasses are often devitrified through controlled thermal annealing[11–13] to obtain a crystalline-amorphous composite aimed at improving the fracture toughness. The art of the heat treatment is again closely related to the thermodynamics of the system in the amorphous and equilibrium states. With this in mind, the phase

MICHAEL C. GAO, Research Associate, formerly with the Department of Materials Science and Engineering, University of Virginia, Charlottesville, VA 22904, is Senior Research Associate, Department of Materials Science and Engineering, Carnegie Mellon University, Pittsburgh, PA 15213. NECIP ÜNLÜ, Research Associate, and G.J. SHIFLET, Professor, are with the Department of Materials Science and Engineering, University of Virginia. Contact e-mail: gjs@virginia.edu MAREK MIHALKOVIC, Visiting Scientist, and MICHAEL WIDOM, Professor, are with the Department of Physics, Carnegie Mellon University, Pittsburgh, PA 15213.

equilibria and the underlying thermodynamics of the Al-rich Al-Fe-Gd[14] system were studied by the current authors using a combined approach of critical experiments and the CALPHAD method. Because there is very limited information on the phase diagrams or the thermochemistry for the Al-TM-RE systems, an experimental phase equilibria study must be performed prior to the CALPHAD modeling.

In parallel to the Al-TM-RE ternary phase diagram study, the Al-RE binaries were also reinvestigated, because most were reported in the 1960s and 1970s and some remain incomplete or unknown.[15,16] In the previous report on the Al-Ce system studied by Gao et al.,[17] it was shown that the $\beta Al_{11}Ce_3$.tI10 compound[15,16] should be treated as Al_4Ce.tI10 based on differential scanning calorimetry (DSC) measurements. (Structures are labeled using the notation {Chemistry}.{Pearson Symbol}, where the chemistry is the chemical formula of the phase of interest.) The differential thermal analysis (DTA) measurements and annealing/quenching tests[17] also suggested a new $AlCe_2$.oP12 phase, but only stable at high temperatures. Further, all the experimental observations and claims made in Reference 17 were supported from FP calculations employing electronic density functional theory.[18] Based on critical experiments and FP calculations, both the Al-Ce and the Al-Nd binary systems were reoptimized and accurate and self-consistent sets of thermodynamic data were achieved.[17] This unique approach combining critical experiments, ab-initio calculations, and CALPHAD modeling provides an effective and accurate way to determine phase diagrams and their corresponding quantitative thermodynamic descriptions. In this report, the same strategy was taken to investigate the Al-rich corner of the Al-Ce-Co ternary system.

II. EXPERIMENTAL PROCEDURES

One hundred and thirty four alloys, many of which are used to identify the glass formation range (GFR), as marked in Figure 1, were synthesized through arc melting pieces of Al (99.999 pct purity), Co (99.9995 pct), and Ce (99.9 pct) on a water-cooled copper hearth using a tungsten electrode in a partial argon atmosphere. Individual ingots were melted 5 to 6 times in total; each time the ingot was flipped over prior to melting to improve homogeneity. The weight loss after melting was found to be less than 1.0 wt pct. All melting and casting of the alloys in a single-wheel melt spinner were done in a He atmosphere to prevent oxidization and improve heat conduction. The wheel was operated at a constant circumferential speed of 48 m/s. Following melt spinning, several experimental techniques including DSC, X-ray diffraction, and transmission electron microscopy (TEM) were used to check whether the as-spun ribbon was amorphous, partial amorphous, or crystalline. This resulted in the GFR, as shown in Figure 1, where earlier reported results[2,19] have also been included.
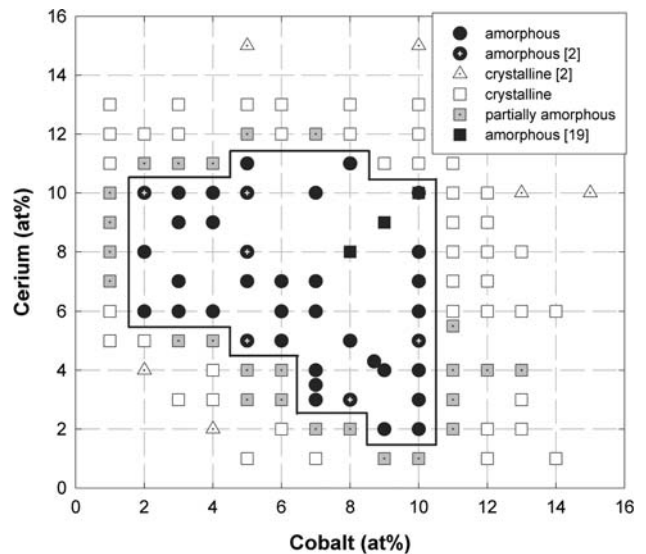

Fig. 1—GFR determined in the Al-rich Al-Ce-Co system, whose border is marked by the solid lines. The early reported work from Refs. 2 and 19 is also shown. The as-quenched alloys were synthesized with a constant circumferential speed of 48 m/s using a single-wheel melt spinning technique.

Thirty-three alloys were selected for the partial 500 °C isotherm study. All the alloys were annealed at 500 °C for 3 weeks under a partial pressure of argon. The annealed samples were quenched into cold water, ground and polished, and finally examined in a LaB_6 and an FEG-scanning electron microscope (SEM) for microstructure analysis. Electron probe microanalysis (EPMA), using pure element samples as external standards, was employed to perform all chemical analysis. The accuracy of the EPMA measurement in this study is about 1 at. pct. The TEM sample preparation was published elsewhere.[13,14]

The DTA measurements were performed on all the 134 arc-melted samples in a Perkin-Elmer (Massachusetts, USA) DTA7 at a heating/cooling rate of 10 K/min up to 1400 °C in a dynamic argon environment. For each sample, the heating/cooling cycle was repeated at least twice to ensure the reproducibility of all the thermal events. The DTA was calibrated with high-purity aluminum and gold with an uncertainty of ± 1 °C on the measured melting points after calibration. All the thermal events during the heating cycles are characterized by the heating onset temperature. The onset is defined by finding the intersection of the baseline and the extrapolated tangent at the inflection point of the leading edge of the peak. However, in certain cases, some thermal events were too weak to give a well-defined onset on heating, but still did show a well-defined cooling onset. In such cases, the peak temperature observed on heating is used.

III. EXPERIMENTAL RESULTS

The GFR determined in this study is shown in Figure 1, together with some earlier reported data.

Alloys with compositions of $Al_{99-y}Ce_yCo_1$ ($y = 8$ to 10, all the composition are in atomic percent unless otherwise specified) were found to be partially amorphous in this study, as opposed to what was reported by Inoue et al.[2] The discrepancy may be due to the difference in the cooling rate employed, e.g., the wheel speed and inert gas used in the chamber. The rationale is that these compositions can be melt spun into amorphous ribbons if a higher cooling rate (i.e., the higher wheel speed) is used. Therefore, the GFR determined in this study is referred to the specific wheel speed of 48 m/s used. Figure 2(a) shows that as-spun $Al_{90}Ce_3Co_7$ is truly amorphous, because no crystalline phase(s) was detected in the dark-field image and the selected area electron diffraction pattern. Figure 2(b) shows that the amorphous alloy completely decomposes into equilibrium phases of fcc-Al, $Al_{11}Ce_3.oI28$, and $Al_9Co_2.mP22$ after annealing at 500 °C for 24 hours.

The experimentally constructed Al-Ce-Co equilibrium 500 °C isotherm is shown in Figure 3 (the 600 °C isotherm assessed by Villars et al. can be found in Reference 20). There are three stoichiometric compounds confirmed, namely, $Al_8CeCo_2.oP44$ (τ_1), Al_4Ce-$Co.oP12$ (τ_2), and $AlCeCo.mC12$ (τ_3). A metastable stoichiometric compound Al_5CeCo_2 (it is proposed to be isostructural with $Al_5CeNi_2.oI16$, based on current FP calculations) was also discovered in the present study (it is not shown in the equilibrium isotherm to avoid confusion). It was found that the Co solubility in the $Al_{11}Ce_3.oI28$ and $\alpha Al_3Ce.hP8$ binary compounds is negligible in agreement with the observation made by Zarechnyul et al.[21] The same is true for Ce solubility in Al-Co binary compounds (not shown). However, the Co solubility in the $Al_2Ce.cF24$ was found to be ~2.5 at. pct Co at 500 °C, while the previously reported Co solubility is ~10 at. pct Co.[21] The solubility limit of Co in Al_2Ce has significant influence on the phase relations and phase tie triangles in its vicinity. Details of the experimental results are presented subsequently.
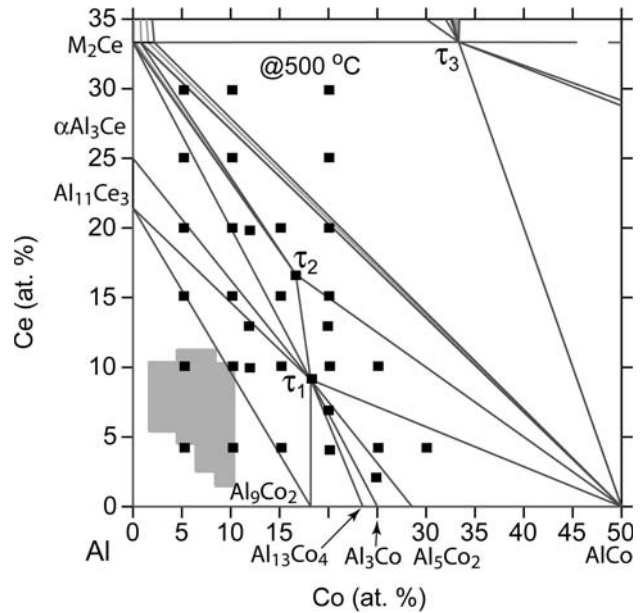

Fig. 3—Al-rich Al-Ce-Co 500 °C isotherm determined in this study. Samples chosen for equilibrium study are marked as filled squares. The shaded area highlights the observed GFR.

The EDX analysis on alloy $Al_{65}Ce_{25}Co_{10}$ (not shown) demonstrates that the Co solubility in $M_2Ce.cF24$ is essentially zero, contradicting Zarechnyul's report of ~5 at. pct.[21] It is concluded that Zarechnyul et al.[21] overestimated the Co solubility in $M_2Ce.cF24$. The EPMA analysis on alloy $Al_{60}Ce_{30}Co_{10}$ showed a Co solubility of ~2.5 at. pct at 500 °C. Therefore, the Co solubility data obtained in the present report is self-consistent and invalidates Zarechnyul's report.[21] Direct evidence on the existence of metastable Al_5CeCo_2 is shown in Figure 4(a). There are four phases present in the microstructure, and all are visible because of the different contrast for each of them and confirmed
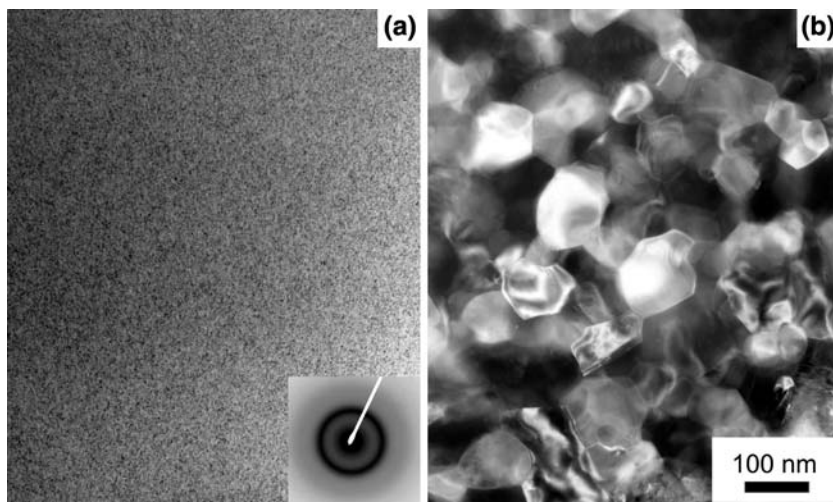

Fig. 2—(a) Dark-field TEM image of the as-spun amorphous alloy $Al_{90}Ce_3Co_7$. The inset is the selected area electron diffraction pattern. (b) Bright-field TEM image of alloy $Al_{90}Ce_3Co_7$ after annealing at 500 °C for 24 hours. The originally amorphous sample was fully crystallized into fcc-Al, $Al_{11}Ce_3$, and Al_9Co_2 phases.
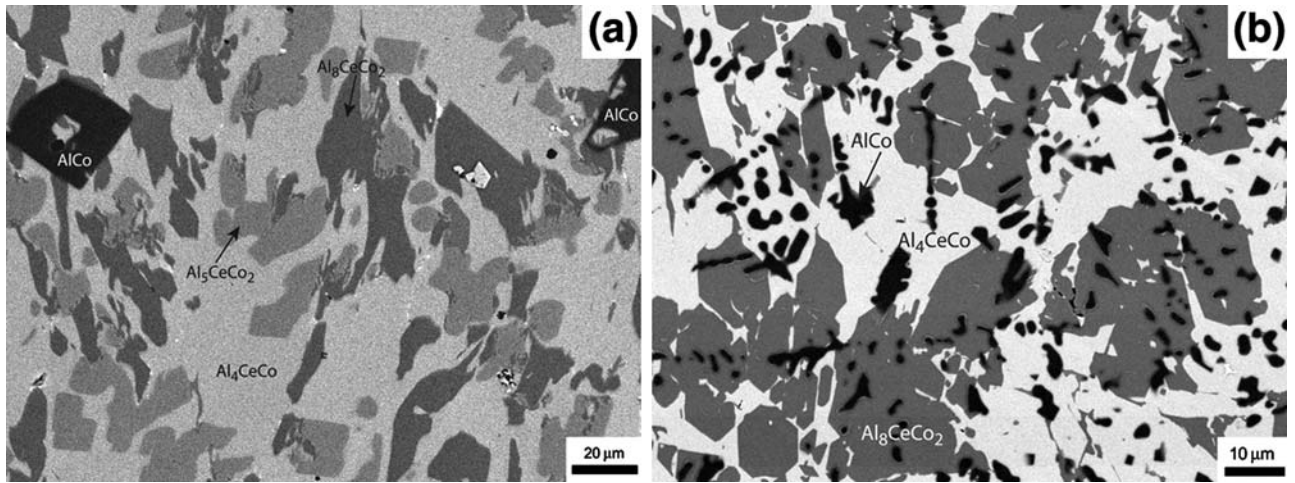
Fig. 4—BSE image of (*a*) alloy $Al_{67}Ce_{13}Co_{20}$ and (*b*) $Al_{65}Ce_{10}Co_{25}$ after annealing at 500 °C for 3 weeks. Note that Al_5CeCo_2.oI16 was not observed in (b), proving that Al_5CeCo_2.oI16 observed in (a) is metastable at 500 °C.
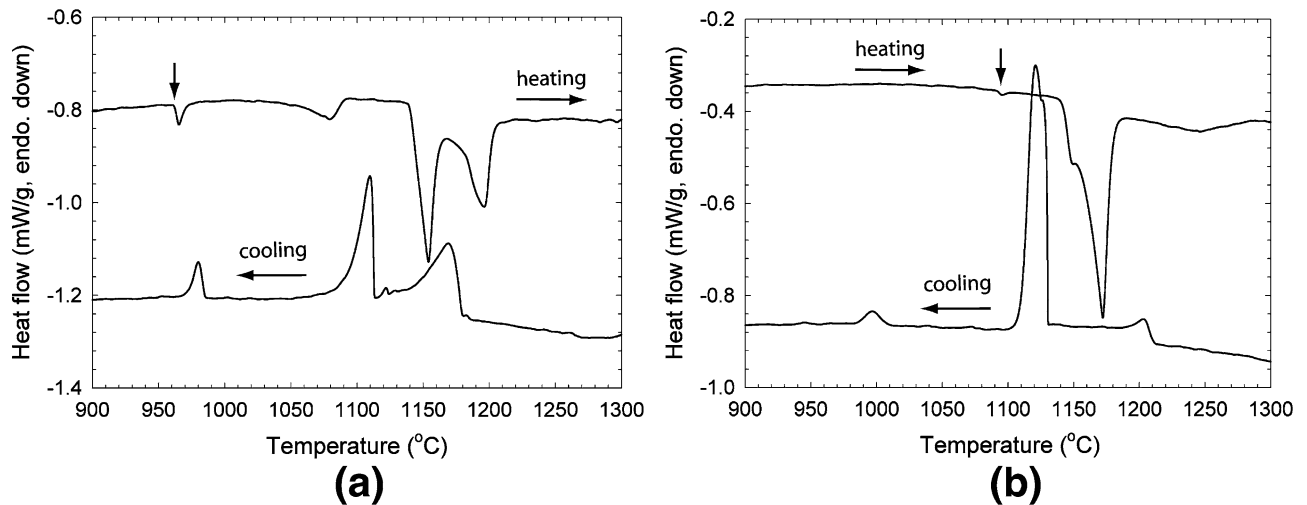

Fig. 5—DTA plots for (*a*) $Al_{75}Ce_{20}Co_5$ and (*b*) $Al_{70}Ce_{20}Co_{10}$. The arrow in (a) marks the onset temperature of the $\alpha/\beta Al_3Ce$ allotropic transition at 961 °C. The arrow in (b) marks the onset temperature of reaction U6: $\beta Al_3Ce + \tau_2 \leftrightarrow M_2Ce + \tau_1$ that occurs at 1089 °C.

by their respective compositional EDX spectra. Because this phase was not observed in another alloy $Al_{65}Ce_{10}Co_{25}$ (Figure 4(b)) nor in alloy $Al_{65}Ce_{25}Co_{10}$ (not shown), it was concluded that Al_5CeCo_2 must be a metastable phase, at least at 500 °C and lower temperatures. A longer annealing at 500 °C or at higher temperatures would be helpful to gain further experimental evidence on its metastability. However, it was not observed in Zarechnyul's 600 °C isotherm experiments.[21]

The overall DTA plots for most of the alloys are complex, which often consist of several thermal events, for example, in alloys $Al_{75}Ce_{20}Co_5$ (Figure 5(a)) and $Al_{70}Ce_{20}Co_{10}$ (Figure 5(b)). It is not immediately possible to identify which phases are involved in each thermal event if only the DTA plot is available. However, this can be done fairly easily once the thermodynamic descriptions for the system are determined (*e.g.*, Figures 7 and 8). Based on the thermody-

namic database developed in this study, the first thermal event with an onset temperature of ~961 °C observed in $Al_{75}Ce_{20}Co_5$ during the heating segment (Figure 5(a)) is concluded to reflect the allotropic transformation of $\alpha/\beta Al_3Ce$, which was recently identified by Gao *et al.*[17] in their Al-Ce binary phase diagram study. This phase transition is also observed in alloy $Al_{75}Ce_{15}Co_{10}$ whose first thermal event has a peak temperature of 970 °C, further confirming the existence of allotropes of $\alpha/\beta Al_3Ce$.[17] The first heating peak in alloy $Al_{70}Ce_{20}Co_{10}$ occurs at 1089 °C (Figure 5(b)), and this event is also observed in several other alloys whose compositions lie within the tie triangles of αAl_3Ce-τ_1-M_2Ce and αAl_3Ce-τ_1-$Al_{11}Ce_3$. Thus, it is concluded that this event must belong to an invariant reaction, and the current thermodynamic calculations actually predict that it results from the phase relation change, namely, $\beta Al_3Ce + \tau_2 \leftrightarrow M_2Ce + \tau_1$ (U_6 in Table IV).

IV. FIRST-PRINCIPLES ENERGY CALCULATION

The Al-Ce-Co ternary system and its constituent binary systems are further analyzed using first-principles (FP) calculations that employ the plane-wave code VASP,[22,23] which solves for the electronic band structure using electronic density functional theory and PAW potentials.[24] Two choices are available for the Ce potential, a "standard" version in which the entire set of f-levels is treated within the valence band and a trivalent version (named "Ce_3") in which some f-electrons are kept frozen in the core. Because the trivalent Ce_3 potential incorrectly predicts a positive enthalpy of formation ($\Delta H_f = +5.7$ kJ/mol)[25] for the stable C15-CeCo2.cF24 compound, the standard Ce potential was used throughout the Al-Ce-Co system. The exchange-correlation functional used is the Perdew–Burke–Ernzerhof (PBE) gradient approximation.[26] Reciprocal space (k-point) meshes are increased and all structures are fully relaxed (both lattice parameters and atomic coordinates) until energies converge to a precision of 1 meV/atom. The plane-wave energy cutoff was held constant at 300 eV, the default for the Ce potential. All calculations were performed using the "Accurate" setting, which avoids wrap-around errors. Spin polarization was considered in all calculations other than pure Al.

To obtain $T = 0$ K enthalpy of formation values ΔH_f, a composition-weighted average of the pure elemental cohesive energies is subtracted from the cohesive energy of a given compound. Stable structures are identified as the vertices of the convex hull of a scatter plot of ΔH_f vs composition. Points above the convex hull represent thermodynamically unstable structures, though they may be metastable or high-temperature stable in some cases. Details of the relaxed structures and their enthalpies can also be found on the worldwide web.[27]

Resulting enthalpies of formation are displayed in Figure 6 for Al-Ce-Co. The lattice stability of Al, Ce, and Co can be found in References 17 and 28. The enthalpy of formation for the Al-Ce binary system was reported in Reference 17. The FP calculations on the Al-Co system are reported in Reference 28. For each pure element, the present calculations correctly identify the low-temperature and known high-temperature phases. For each binary and the ternary, however, disagreements are found between the calculated phase diagrams and the experimentally established ones. Some of the disagreements probably reflect poor approximations made in the calculated cohesive energies, for example, the use of nonrelativistic quantum mechanics. Other, stronger disagreements require further study, both theoretical and experimental. The binary diagrams are fairly well reproduced, but the agreement in the case of Al-Ce is less impressive than in other studies of non-RE-containing alloys.[29] The binary Al-Ce phase diagram was already discussed in Reference 17.

Binary Al-Co exhibits several interesting structures in the Al-rich region. Experimental investigation of the phase diagram is ongoing, with the greatest uncertainty
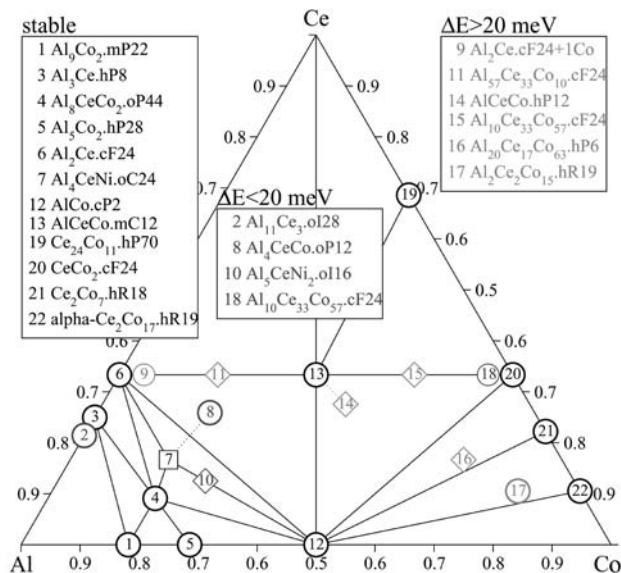

Fig. 6—Convex hull and metastable/unstable phases of the Al-Ce-Co system. The plotting symbol notation is as follows: heavy circles for known stable binary phases; light circles for known high-temperature phases; diamonds for known metastable phases; triangles for known high-pressure phases; and squares for imperfectly known, unknown, or hypothetical structures. Tie-lines run along convex hull edges, joining low enthalpy structures at the vertices of the convex hull.

in the composition range $Al_{13}Co_4$-Al_3Co, where a variety of "quasi-crystal approximant" structures are observed.[30–34] The well-known stable phases Al_9Co_2.mP22 and Al_5Co_2.hP28 are found on either side of this problematic composition range. Further discussion of the composition range $Al_{13}Co_4$-Al_3Co may be found in Reference 28.

The Ce-Co yields excellent agreement with the established phase diagram provided the standard Ce potential is used, as opposed to trivalent Ce_3 in which the f-level is kept frozen. The calculated enthalpy of formation and lattice parameters are listed in Table I, and the latter agree with experimentally determined values. The cluster of reported stable phases from $CeCo_3$ to Ce_5Co_{19} is thermodynamically implausible, and the present calculation is more consistent with a single low-temperature phase (possibly Ce_2Co_7) together with two high-temperature or metastable phases on either side of it. The hP6 structure of $CeCo_5$ is properly identified as a high-temperature phase.

The ternary diagram is well reproduced. The enthalpies of formation data set for stable and hypothetical compounds are listed in Table II together with the calculated lattice parameters, which closely agree with the experimentally determined values. The known stable phases that are confirmed are as follows: Al_8CeCo_2.oP44, which is recognized as a decagonal quasi-crystal approximant,[21,35] and AlCeCo.mC12. The alternate reported structure AlCeCo.hP12 is high in energy by 144 meV/atom and most likely is metastable. At the composition of Al_4CeCo.oP12, a different structure was found, namely, Al_4CeNi.oC24 lower in energy by 5 meV/atom. Because it was not possible to perfectly

Table I. Enthalpies of Formation of Stable Compound Phases, ΔH_f, at $T = 0$ K for the Ce-Co System Calculated by FP and a Comparison of Calculated Lattice Parameters with Experimental Data

| | | | Lattice Parameters (Å) | | | |
| | | | Ab Initio (This Work) | | Experiment[62] | |
Compound*	Pearson Symbol-Prototype	ΔH_f (kJ/mol of atoms)	a	c	a	c
$^{s}Ce_{24}Co_{11}$	$hP70$-$Ce_{24}Co_{11}$	−13.46	9.351	20.814	9.587	21.825
$^{s}CeCo_2$	$cF24$-Cu_2Mg	−24.09	7.058	—	7.160	—
$^{lt}\alpha Ce_2Co_{17}$	$hR19$-Th_2Zn_{17}	−8.23	8.318	12.119	8.378	12.206
$^{ht}\beta Ce_2Co_{17}$	$hP38$-Th_2Ni_{17}	−7.75	8.315	8.080	8.378	8.1317
$^{s}Ce_5Co_{19}$	$hR24$-Ce_5Co_{19}	−15.2	4.872	49.148	4.948	48.7434
$^{s}CeCo_3$	$hR12$-Be_3Nb	−17.44	4.887	24.900	4.964	24.814
$^{ht}CeCo_5$	$hP6$-$CaCu_5$	−10.41	4.876	4.022	4.920	4.029
$^{s}Ce_2Co_7$	$hR18$-Co_7Er_2	−16.67	4.882	37.103	4.940	36.52

*s: stable, lt: low-temperature phase, and ht: high-temperature phase.

Table II. Enthalpies of Formation of Ternary Compound Phases, ΔH_f (kJ/mol of Atoms), at $T = 0$ K for Al-Ce-Co System Calculated by FP; the Deviation from the Convex Hull (kJ/mol of Atoms) is Marked as ΔE; the Calculated Lattice Parameter is Also Shown in Comparison with the Available Experimental Data

| | | | | Lattice Parameters (Å) | | | | | |
| | | | | Ab Initio (This Work) | | | Experiment[62] | | |
Phase*	Pearson Symbol-Prototype	ΔH_f	ΔE	a	b	c	a	b	c
$^{s}Al_8CeCo_2$	$oP44$-Al_8CeCo_2	−46.26	0.0	14.357	12.389	3.994	14.30	12.41	4.12
$^{s}Al_4CeCo$	$oP12$-Al_4CeCo	−47.63	0.5	7.594	4.041	6.791	7.59	4.048	7.014
$^{s}AlCeCo$	$mC12$-$AlCeCo$	−50.51	0.0	11.066	4.429	4.726	11.098	4.410	4.807
				α,γ = 90 deg; β = 106.44 deg			α,γ = 90 deg; β = 104.61 deg		
$^{h}Al_4CeCo$	$oC24$-Al_4CeNi	−48.12	0.0	4.094	15.506	6.648	—	—	—
$^{h}AlCeCo$	$hP9$-$AlNdNi$	−46.34	4.2	6.824	—	4.011	—	—	—
$^{h}AlCeCo$	$hP12$-$AlCeCo$	−36.61	13.9	5.461	—	8.300	—	—	—
$^{h}Al_3CeCo$	$oP20$-Al_3NiY	−48.22	1.9	8.130	4.031	10.770	—	—	—
$^{h}Al_8CeCo_4$	$tI26$-Al_8CeFe_4	−47.71	4.1	8.588	—	5.109	—	—	—
$^{m}Al_5CeCo_2$	$oI16$-Al_5CeNi_2	−48.88	1.5	7.130	9.334	3.947	—	—	—
$^{h}Al_7Ce_6Co_7$	$tP40$-$Al_7Co_6Pr_7$	−44.54	4.3	13.175	—	4.289	—	—	—
$^{u}Al_2Ce_2Co_{15}$	$hR19$-$Al_2Ce_2Co_{15}$	−16.16	4.3	8.355	—	12.283	8.44	—	12.30

*s: stable, h: hypothetical, m: metastable, and u: unstable.

reproduce the Al-Ce binary diagram, it is difficult to assert which structure is the true low energy state. Rather, further experimental and theoretical effort is required to resolve the matter. Finally, it was found that Al_5CeNi_2.oI16 has a low energy of only 15 meV/atom, indicating a possible metastable or high-temperature phase. This is possibly the structure for a metastable phase obtained in the experimental portion of this work.

Further calculations were performed to examine the composition ranges of all Al-Ce and Ce-Co binary structures as they extend into the ternary through substitutions of Al and Co atoms. All substitutions were found to be highly unfavorable, with the highest concentration (i.e., lowest energy) found in the case of $CeCo_2$. For this compound, the substitution energy is found to be ΔE = 0.36 eV. At T = 500 K, the thermal energy k_BT = 0.043 eV, so it is estimated that a fraction exp (−0.36 eV/0.043 eV) = 0.002 of the Al atoms will

be substituted by Al atoms. This behavior differs markedly from an alloy such as Al-Ca-Cu, where Al and Cu easily substitute for each other.[36] Evidently, the filled d-level of the noble metal Cu lets it more easily substitute for Al than is the case for the transition metal Co, with its partially filled d-level.[37]

V. THERMODYNAMIC MODELS

The Gibbs free energy of individual phases is described by sublattice models[38] and is defined relative to the standard element reference (SER), i.e., the enthalpies of the pure elements in their defined reference phase at 298.15 K and 1 atm. All the disordered solutions including the liquid are modeled with a single sublattice, with the Gibbs energy expressed as for a ternary complete disordered solution (e.g., liquid) with components Al, Ce, and Co:

$$G^{\phi} = \sum_{i=\text{Al,Ce,Co}} x_i \, {}^oG_i^{\phi} + RT \sum_{i=\text{Al,Ce,Co}} x_i \ln x_i$$
$$+ {}^{ex}G_{\text{Al,Ce,Co}}^{\phi} + {}^{mag}G_{\text{Al,Ce,Co}}^{\phi} \qquad [1]$$

where $^oG_i^{\phi}$ is the molar Gibbs energy of the pure element i in the structure of phase ϕ in the nonmagnetic state, taken from the values tabulated by Dinsdale,[39] and x_i is the mole fraction of each component. (The colon in the subscript is used to separate different sublattices, while the comma indicates solid solution.) The excess Gibbs energy, $^{ex}G_{\text{Al,Ce,Co}}^{\phi}$, is expressed in Redlich–Kister–Muggianu polynomial form:[40,41]

$$^{ex}G_{\text{Al,Ce,Co}}^{\phi} = x_{\text{Al}}x_{\text{Ce}} \sum_{k=0}^{k} {}^kL_{\text{Al,Ce}}^{\phi}(x_{\text{Al}} - x_{\text{Ce}})^k$$
$$+ x_{\text{Ce}}x_{\text{Co}} \sum_{k=0}^{k} {}^kL_{\text{Ce,Co}}^{\phi}(x_{\text{Ce}} - x_{\text{Co}})^k$$
$$+ x_{\text{Al}}x_{\text{Co}} \sum_{k=0}^{k} {}^kL_{\text{Al,Co}}^{\phi}(x_{\text{Al}} - x_{\text{Co}})^k$$
$$+ x_{\text{Al}}x_{\text{Ce}}x_{\text{Co}} \left({}^0L_{\text{Al,Ce,Co}}^{\phi}x_{\text{Al}} + {}^1L_{\text{Al,Ce,Co}}^{\phi}x_{\text{Ce}} \right.$$
$$\left. + {}^2L_{\text{Al,Ce,Co}}^{\phi}x_{\text{Co}} \right) \qquad [2]$$

where $^kL_{i,j}^{\phi}$ where $^kL_{i,j}^{\phi}$ are the binary interaction parameters (k is an integer), which are taken directly from individually assessed edge binary databases; and $^kL_{\text{Al,Ce,Co}}^{\phi}$ are the ternary interaction parameters, which are to be optimized in this study. Both the binary and ternary interaction parameters have the following general form:

$$^kL^{\phi} = {}^ka + {}^kbT + {}^kcT\ln\,(T) + {}^kdT^2 + {}^keT^{-1} + {}^kfT^{-3} \qquad [3]$$

The magnetic contribution to the Gibbs energy ($^{mag}G^{\phi}$) for all the ternary compound phases in the Al-rich corner was set to zero, because they all order at very low temperatures less than 100 K. It is only significant for the Ce-Co binary and Co-rich ternary alloys, neither of which are the focus of this study.

Stoichiometric compounds are modeled as if the enthalpy and entropy are constants and only one element occupies one sublattice. For example, the Gibbs free energy for a ternary stoichiometric compound $\text{Al}_x\text{Ce}_y\text{Co}_z$ (x, y, and z denote the chemical formula) is modeled as (J/mole of total atoms)

$$G^{\text{Al}_x\text{Ce}_y\text{Co}_z} = \frac{x}{x+y+z}{}^oG_{\text{Al}}^{\text{fcc}}$$
$$+ \frac{y}{x+y+z}{}^oG_{\text{Ce}}^{\text{fcc}} + \frac{z}{x+y+z}{}^oG_{\text{Co}}^{\text{hcp}} + a + bT \qquad [4]$$

where a and b are the parameters to be determined, namely, the enthalpies of formation and entropies of formation for the compound $G^{\text{Al}_x\text{Ce}_y\text{Co}_z}$, respectively.

The terms $^oG_{\text{Al}}^{\text{fcc}}$, $^oG_{\text{Ce}}^{\text{fcc}}$, and $^oG_{\text{Co}}^{\text{hcp}}$ are the Gibbs energies of the pure components, Al, Ce, and Co, with respect to its enthalpies in the SER state, respectively. Note that both Ce and Co have several allotropes in the solid state. At the SER state, both Al and Ce have a crystal structure of fcc, while Co has a crystal structure of hcp.

The Gibbs energy of those binary $(\text{Al,Co})_x\text{Ce}_y$ compound phases that have ternary solubility (i.e., Al and Co substitute for each other in ternary phase) is expressed as

$$G^{(\text{Al,Co})_x\text{Ce}_y} = \sum_{i=\text{Al,Co}} y_i \, {}^oG_{i:\text{Ce}}^{(\text{Al,Co})_x\text{Ce}_y} + \frac{x}{x+y}RT \sum_{i=\text{Al,Co}} y_i \ln y_i$$
$$+ y_{\text{Al}}y_{\text{Co}} \sum_{k=0}^{k} {}^kL_{\text{Al,Co:Ce}}^{(\text{Al,Co})_x\text{Ce}_y}(y_{\text{Al}} - y_{\text{Co}})^k \qquad [5]$$

where $^kL_{\text{Al,Co:Ce}}^{(\text{Al,Co})_x\text{Ce}_y}$ are the interaction parameters and have a form in Eq. [3]. The $^oG_{\text{Al:Ce}}^{(\text{Al,Co})_x\text{Ce}_y}$ and $^oG_{\text{Co:Ce}}^{(\text{Al,Co})_x\text{Ce}_y}$ represent the Gibbs energy of the compound Al_xCe_y and Co_xCe_y, respectively. These two expressions were obtained from the binary assessments without change during optimization. Only the interaction term $^kL_{\text{Al,Co:Ce}}^{(\text{Al,Co})_x\text{Ce}_y}$, which contains a series of parameters a, b, c... (Eq. [3]), was optimized in this study to obtain best fitting between the calculated phase diagram and experimental data achieved in this study and those assessed in Reference 21. It was found in Reference 21 and the present study that in the Al-rich corner, only Al₂Ce.cF24 extends into ternary solubility, but CeCo₂.cF24 also has significant ternary solubility.[21] Therefore, both are treated as one ternary phase M₂Ce (M = Al, Co) with a two-sublattice model of $(\text{Al,Co})_2(\text{Ce})_1$. This choice makes physical sense, because (1) both Al₂Ce and CeCo₂ are A₂B-type Laves phases (prototype Cu₂Mg, Pearson symbol cF24), and their lattices consist of only two crystallographic sites (A atoms occupy Wyckoff sites 16d and B atoms occupy 8a); and (2) substitution between Al and Co in the 16d site is energetically favored and is confirmed, while substitution between Al/Co and Ce in the 8a site is not found in Reference 21 and this study.

The Al-Co system was thermodynamically optimized by Dupin and Ansara,[42] and their thermodynamic descriptions were directly used without modification. The stable intermetallic compounds reported for the Al-Co binary system include Al₉Co₂.mP22, Al₁₃Co₄.mC32, Al₃Co.oP16, Al₅Co₂.hP28, and AlCo.cP2.

The Ce-Co binary was thermodynamically assessed by Su et al.,[43] and two different approaches were offered in the assessment. The first one treated both Ce₂Co₁₇ and CeCo₅ as stoichiometric compounds, and the CeCo₅.hP6 transforms into Ce₅Co₁₉ and Ce₂Co₁₇ via eutectoid reaction. The other treatment treated Ce₂Co₁₇ and CeCo₅ as a single phase with different compositions, and CeCo₅.hP6 transforms into Ce₅Co₁₉.hR24 and Ce₂Co₁₇.hR19 via spinodal decomposition, as suggested in Reference 44. However, the second one remains controversial, as argued in Reference 45. In the established Ce-Co phase diagram,[15,16] several compounds

with close chemistry ($CeCo_3$, Ce_2Co_7, and Ce_5Co_{19}) coexist stably up to high temperatures, violating the empirical thermodynamic rule[16] stating that two compounds with close chemistry should not both be stable over a wide temperature range. This implies that it is likely some compound phases reported in the Ce-Co system may be metastable or only stable for temperature ranges. Recall that the present FP calculations suggest that only Ce_2Co_7 is stable at low temperatures. Considering all the uncertainties in the Ce-Co system, the first treatment in Reference 43 was taken without alteration, because the Al-rich corner is the focus of this report. Clearly, further careful experiments are needed to clarify all the confusion in the Ce-Co phase diagram.

The thermodynamics of the Al-Ce system was assessed previously by Cacciamani et al.[46] and recently by Gao et al.[17,25] Because Gao et al.[17] confirmed the $Al_4Ce.tI10$ as stable, opposing the previously claimed $\beta Al_{11}Ce_3$.-tI10,[15,16] and Gao et al.[17] also confirmed a new phase $AlCe_2.oP12$ stable at high temperature, the thermodynamic description of Reference 17 for the Al-Ce system was accepted for the Al-Ce-Co system. The $Al_2Ce.cF24$ was treated as a stoichiometric compound.[17] The descriptions for the hypothetical C15 end members and antilattice are provided in Reference 25.

The Al-Ce-Co ternary phase diagram assessed in Reference 20 is mainly based on the work by Zarechnyul et al.[21] in 1980, who constructed the partial 600 °C isotherm in the range of 0 to 33.3 at. pct Ce. The ternary stoichiometric compounds assessed in Reference 20 include $Al_8CeCo_2.oP44$,[21] $Al_4CeCo.oP12$,[21] Al_2Ce_2-$Co_{15}.hR19$,[47] $Al_4Ce_3Co_3.oP$[48] (the atomic position was not reported in Reference 48), $AlCeCo.hP12$,[49] and $AlCeCo.mC12$.[50] In addition, Zarechnyul et al.[21] found three binary compounds that show ternary solubility between Al and Co atoms at 600 °C. Specifically, Co solubility in $Al_2Ce.cF24$ is ~10 at. pct Co, Al solubility in $CeCo_2.cF24$ is ~10 at. pct Al, and Al solubility in $CeCo_5.hP6$ is ~20 at. pct Al.

VI. MODELING RESULTS AND DISCUSSION

The Thermo-Calc package[51] is used to optimize the ternary system using the PARROT module. The opti-mization is based on the experimental data from this study, such as DTA measurements, phase relationships, phase compositions, and phase crystal structures. It is usually difficult to obtain the liquidus temperatures accurately, and, furthermore, rare earth elements are susceptible to oxidation. Thus, the liquidus data are assigned with lower weight during optimization. In contrast, the invariant reaction temperatures are seen to be reproducible and thus more reliable, and they are set with higher weight during the global optimization. The thermodynamic parameters obtained in this study are listed in Table III. Figure 7 shows the calculated partial isopleths (vertical sections) through the Al-Co-Ce phase diagram at fixed Ce contents of 4 and 10 at. pct. Isopleths at fixed Co contents of 5 and 10 at. pct are shown in Figure 8. These figures illustrate how alloy compositions and temperature affect the equilibrium phase diagrams and demonstrate that the phase transformations during equilibrium solidification for compositions within the GFR are complicated. Figures 7 and 8 also show that the agreement is excellent between calculated phase transition temperatures and experimental DTA data. For other compositions whose DTA measurements were performed in this study, good agreement is also obtained.

Note that current thermodynamic descriptions predict that a reaction of $\beta Al_3Ce + \tau_2 \leftrightarrow M_2Ce + \tau_1$ (Table IV) occurs at ~1090 °C, and consequently the composition triangle relationship among τ_1, τ_2, βAl_3Ce, and M_2Ce changes when the temperature is raised from 1000 °C to 1100 °C. This is not common because there is no additional solid phase formation, and no liquid is yet formed at these temperatures for both composition triangles. Surprisingly, the predicted invariant temperature for the reaction of $\beta Al_3Ce + \tau_2 \leftrightarrow M_2Ce + \tau_1$ agrees extremely well with the DTA thermal events at ~1089 °C recorded for alloys $Al_{70}Ce_{25}Co_5$ and $Al_{70}Ce_{20}$-Co_{10} during heating segment (the DTA plots in Figure 5 and the thermal events marked in Figure 8).

A calculated liquidus surface projection with liquidus isocontours is presented in Figure 9. The solid lines refer to the univariant equilibria between the liquid and two solid phases, and three lines intersect at an invariant reaction point where four phases coexist at equilibrium.

Table III. Thermodynamic Parameters Obtained in the Present Study

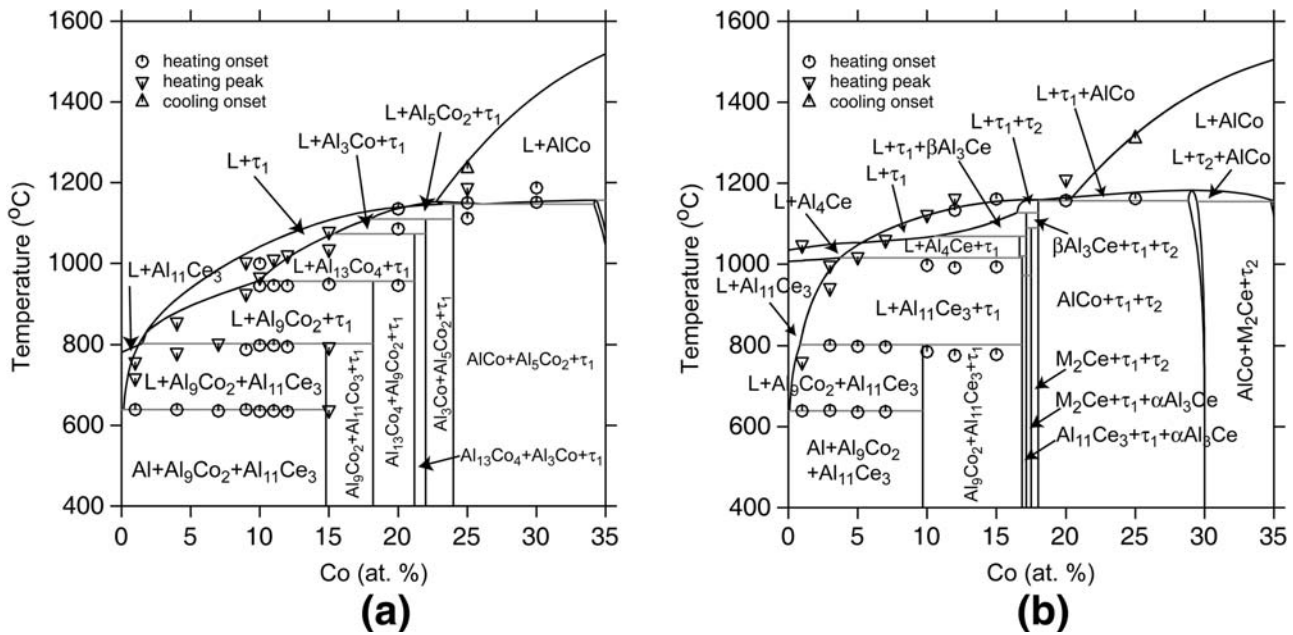| Phase	Parameter (J/mol of Atoms)
Liquid	$^0L_{Al,Ce,Co}^{liq} = +74{,}439 - 3.053T$
	$^1L_{Al,Ce,Co}^{liq} = -90{,}050 + 1.943T$
	$^2L_{Al,Ce,Co}^{liq} = +84{,}638 + 6.757T$
$(Al,Co)_2Ce$	$^0L_{Al,Co:Ce}^{(Al,Co)_2Ce} = -26423 + 5.257T$
	$^1L_{Al,Co:Ce}^{(Al,Co)_2Ce} = +500$
	$^2L_{Al,Co:Ce}^{(Al,Co)_2Ce} = +5.0T$
Al_8CeCo_2 (τ_1)	
	$G_{Al:Ce:Co}^{\tau_1} = 811 {}^o G_{Al}^{fcc} + 111 {}^o G_{Ce}^{hcp} + 211 {}^o G_{Co}^{fcc} - 52{,}223 + 13.744T$
Al_4CeCo (τ_2)	$G_{Al:Ce:Co}^{\tau_2} = 46 {}^o G_{Al}^{fcc} + 16 {}^o G_{Ce}^{hcp} + 16 {}^o G_{Co}^{fcc} - 54{,}802 + 12.705T$
$AlCeCo$ (τ_3)	$G_{Al:Ce:Co}^{\tau_3} = 13 {}^o G_{Al}^{fcc} + 13 {}^o G_{Ce}^{hcp} + 13 {}^o G_{Co}^{fcc} - 54{,}296 + 8.146T$

Fig. 7—Calculated isopleth plot of (a) Al-4Ce-Co and (b) Al-10Ce-Co from the thermodynamic descriptions obtained in the present work.
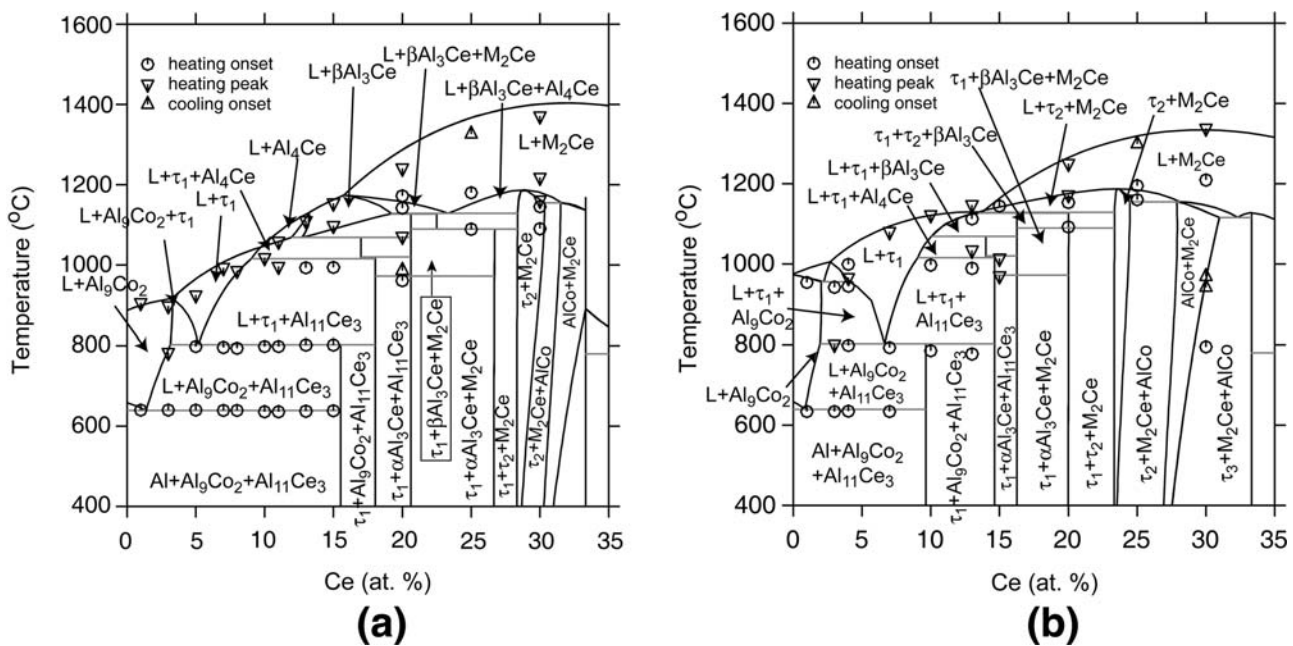

Fig. 8—Calculated isopleth plots of (a) Al-Ce-5Co and (b) Al-Ce-10Co from the thermodynamic descriptions obtained in the present work.

All the invariant reactions involving the liquid (Figure 9) are listed in Table IV. The majority of the predicted invariant reaction temperatures agree exceptionally well with DTA measurements except for a few reactions including U_3, U_8, and U_7 whose agreement is imperfect. For reaction U_3 ($Al_4Ce + \tau_1 \leftrightarrow L + Al_{11}Ce_3$), the current model slightly overestimated the reaction temperature but is still acceptable. This is thought to be due to possible stabilization of the $Al_4Ce.tI10$ by impurity or minor solute effects. In order

to greatly improve agreement with the measured DTA data, the current authors then take a sublattice model of $(Al,Co)_4(Ce)_1$ to model the Al_4Ce phase, i.e., to allow Co atoms to mix with Al atoms. The resulting optimization finds that the agreement of U_3 with experiments cannot be improved substantially unless a significant Co solubility (≥ 10 at. pct) in Al_4Ce is used, which, however, contradicts the present FP prediction that shows that Al/Co substation in the ternary is very limited. Therefore, this treatment is not progressed further and is not

Table IV. Invariant Reactions Obtained in the Present Study

Sym.	T (°C) Cal.	T (°C) Exp.	$X(L$, At. Pct) Co	Ce	Reaction*
E_1	639	640	0.2	1.9	$L \leftrightarrow Al_{11}Ce_3 + Al_9Co_2 + Al$
U_1	803	798	1.3	4.1	$L + \tau_1 \leftrightarrow Al_{11}Ce_3 + Al_9Co_2$
U_2	955	945	7.6	2.6	$L + Al_{13}Co_4 \leftrightarrow \tau_1 + Al_9Co_2$
U_3	1015	996	4.1	9.0	$Al_4Ce + \tau_1 \leftrightarrow L + Al_{11}Ce_3$
U_4	1068	1073	5.9	10.5	$L + \beta Al_3Ce \leftrightarrow Al_4Ce + \tau_1$
U_5	1073	1085	14.6	2.6	$L + Al_3Co \leftrightarrow Al_{13}Co_4 + \tau_1$
U_6	1090	1089	—	—	$\beta Al_3Ce + \tau_2 \leftrightarrow M_2Ce + \tau_1$
U_7	1110	1135	17.9	2.8	$L + Al_5Co_2 \leftrightarrow Al_3Co + \tau_1$
E_2	1116	—	21.1	28.6	$L \leftrightarrow AlCo + M_2Ce + \tau_3$
U_8	1127	1143	9.7	13.6	$L + \tau_2 \leftrightarrow \beta Al_3Ce + \tau_1$
U_9	1128	—	9.7	13.7	$L + M_2Ce \leftrightarrow \tau_2 + \beta Al_3Ce$
U_{10}	1147	1151	22.2	4.8	$L + AlCo \leftrightarrow Al_5Co_2 + \tau_1$
U_{11}	1155	1162	19.6	21.5	$L + \tau_2 \leftrightarrow AlCo + M_2Ce$
E_3	1156	1159	20.6	9.0	$L \leftrightarrow AlCo + \tau_1 + \tau_2$
U_{12}	1192	—	2.8	16.6	$L + M_2Ce \leftrightarrow Al_4Ce + \beta Al_3Ce$

*The phases on the left-hand side are higher-temperature phases, and those on the right-hand side are lower-temperature phases.

presented here. For reactions U_8 ($L + \tau_2 \leftrightarrow \beta Al_3Ce + \tau_1$) and U_9 ($L + M_2Ce \leftrightarrow \tau_2 + \beta Al_3Ce$), their reaction temperature and liquid composition are so close to each other that their thermal events overlap during DTA measurements. This makes precise determination of the onset temperature for each reaction difficult. For reaction U_7 ($L + Al_5Co_2 \leftrightarrow Al_3Co + \tau_1$), the uncertainty in reaching equilibrium state for Al_3Co and Al_5Co_2[30–34] may be responsible for the imperfect agreement on the reaction temperature with DTA measurement.

The liquidus surface projection and isocontours (Figure 9) show that increasing Ce or Co contents in the alloy monotonically raises the liquidus temperature (beyond the ternary eutectic point E_1), and the compositions within the GFR have liquidus temperatures that lie between ~900 °C and ~1125 °C. The ternary τ_1 compound has the broadest primary compositional field in the Al-rich corner, so it is mainly responsible for the liquidus temperature of alloys within the GFR, and thus impacts the glass formation the most. On the other hand, the ternary τ_2 compound has less impact on the glass formation, and the primary τ_2 phase field has a nearly plateau liquidus temperature of 1175 °C. Further, the observed GFR is very narrow and is mainly limited by the wide phase fields of the primary M_2Ce and AlCo, which both are very stable in the edge binaries and the ternary and impact the ternary phase equilibria substantially. In order to improve the GFA and broaden the GFR in the Al-Ce-Co system, an alloying strategy could be sought to lower the melting point of the ternary τ_1 compound and destabilize M_2Ce and AlCo solution compounds as one effective measure.

Previous work by Gao et al.[17] showed that (1) a polymorphous transition of $\beta Al_3Ce \leftrightarrow \alpha Al_3Ce$ occurs at ~973 °C and (2) a catetectic $Al_4Ce \leftrightarrow L + Al_{11}Ce_3$ occurs at 1006 °C in the Al-Ce binary. For the Al-Ce-Co ternary, the $\alpha/\beta Al_3Ce$ transition temperature measured in this study is found to fluctuate slightly, i.e.,

961 °C to 970 °C, but fairly close to that in the binary, i.e., ~973 °C (Figure 7 and the first thermal event marked for alloys $Al_{75}Ce_{20}Co_5$ and $Al_{75}Ce_{15}Co_{10}$ in Figure 8). Therefore, it is further confirmed that the polymorphism of $\alpha/\beta Al_3Ce$ exists in the Al-Ce system.[17] The slight decrease in the $\alpha/\beta Al_3Ce$ transition temperature in the Al-Ce-Co ternary may be due to the possibility of small Co solid solution in βAl_3Ce or other unidentified reasons. Due to lack of direct measurement of relevant Co solubility data, this possibility is not considered in the current thermodynamics modeling. On the other hand, the binary catetectic reaction of $Al_4Ce \leftrightarrow L + Al_{11}Ce_3$ becomes the reaction of $Al_4Ce + \tau_1 \leftrightarrow L + Al_{11}Ce_3$ in the Al-Ce-Co ternary that occurs at 996 °C ± 6 °C. Such a change in the reaction temperature provides further experimental support that the phase transition between Al_4Ce and $Al_{11}Ce_3$ cannot be polymorphous.[17]

The present study indicates that reliable CALPHAD modeling can be used to interpret DTA measurements with high confidence. This is useful because there are often several thermal events for each alloy (Figures 5, 7, and 8), and it is not possible to immediately determine the reaction type (i.e., eutectic, eutectoid, etc.) and exact phases involved in each thermal event for each alloy if only the DTA plot is available. The thermodynamics of Al-Ce-Co in the present work are determined through the classical CALPHAD approach, and the values of the formation enthalpies of the ternary compounds (Table III) through the CALPHAD optimization scheme are found to be comparable with those from FP calculations (Table I). In fact, employment of FP calculations into phase diagram studies and further integration of FP calculations into CALPHAD modeling have become very active and important in the community of phase diagram research. Clearly, integrating FP calculations into phase diagram research will play an indispensable role especially for the multicomponent system, in addition to critical experiments and CALPHAD modeling.[13,29,52–61]
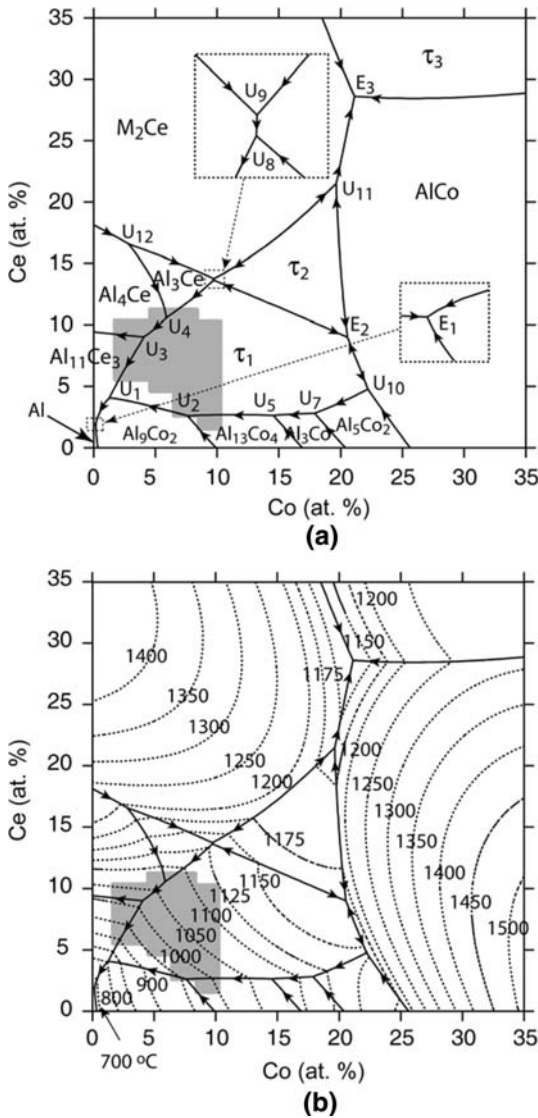
Fig. 9—(a) liquidus surface projection and (b) liquidus isocontours calculated from the thermodynamic descriptions obtained in the present work. The solid lines are univariant equilibria and the primary crystallization phase field is labeled. The dotted lines are the liquidus isotherms, and the arrows indicate the downward temperature gradient. The shaded area represents the GFR identified in the present work.

VII. CONCLUSIONS

The Al-rich Al-Ce-Co system was investigated using a range of experimental techniques and FP energy calculation, reaching the following new conclusions.

1. The GFR was determined using a constant circumferential speed of 48 ms^{-1}. It is slightly narrower than reported by Inoue et al.,[2] and the slight disagreement is probably a result of the different quenching rate or quenching environment used.
2. There are three stoichiometric compounds confirmed, namely, $Al_8CeCo_2.oP44$ (τ_1), $Al_4CeCo.oP12$ (τ_2), and $AlCeCo.mC12$ (τ_3).
3. A metastable stoichiometric compound with a composition of Al_5CeCo_2 was discovered, and its structure is likely to be isostructural with $Al_5CeNi_2.oI16$, as suggested by FP calculations.
4. This investigation further confirmed the earlier statements by Gao et al.[17] that (a) a polymorphous transformation of $\alpha/\beta Al_3Ce$ exists in the Al-Ce binary system; and (b) the transformation between $Al_{11}Ce_3.oI28$ and $Al_4Ce.tI10$ cannot be polymorphous, disagreeing with the assessed phase diagram handbooks.[15,16]
5. The Co solubility in the $Al_2Ce.cF24$ was found to be ~2.5 at. pct at 500 °C, which is significantly smaller than reported by Zarechnyul et al.[21] The phase relation in its vicinity was revised accordingly.
6. The FP calculations show that none of the Al-Ce binary compounds has extended Co solubility into the ternary at high temperatures. The enthalpy penalty for Al/Co mixing is too high to be compensated by the entropy gain.
7. The Al-rich Al-Ce-Co system was thermodynamically optimized for the first time. Agreement between the calculated phase boundary and DTA data is obtained. The enthalpies of formation for the ternary compounds obtained from CALPHAD modeling are comparable to those from FP calculations.

REFERENCES

1. Y. He, S.J. Poon, and G.J. Shiflet: *Science*, 1988, vol. 241, pp. 1640–42.
2. A. Inoue, K. Ohtera, A.P. Tsai, and T. Masumoto: *Jpn. J. Appl. Phys. Lett.*, 1988, vol. 27, pp. L280–L282.
3. W.L. Johnson, A. Inoue, and C.T. Liu: *Bulk Metallic Glasses*, Materials Research Society Symposia Proceedings, MRS, Warrendale, PA, 1999, vol. 554.
4. D.B. Miracle, W.S. Sanders, and O.N. Senkov: *Phil. Mag.*, 2003, vol. 83, pp. 2409–28.
5. F.Q. Guo, S.J. Poon, and G.J. Shiflet: *Appl. Phys. Lett.*, 2004, vol. 84, pp. 37–39.
6. N. Saunders and A.P. Miodownik: *Mater. Sci. Technol.*, 1988, vol. 4, pp. 768–77.
7. X.H. Lin and W.L. Johnson: *J. Appl. Phys.*, 1995, vol. 78, pp. 6514–9.
8. X.P. Tang, U. Geyer, R. Busch, W.L. Johnson, and Y. Wu: *Nature*, 1999, vol. 402, pp. 160–2.
9. F. Faupel, W. Frank, M.P. Macht, H. Mehrer, V. Naundorf, K. Ratzke, H.R. Schober, S.K. Sharma, and H. Teichler: *Rev. Mod. Phys.*, 2003, vol. 75, pp. 237–80.
10. R. Busch, Y.J. Kim, and W.L. Johnson: *J. Appl. Phys.*, 1995, vol. 77, pp. 4039–43.
11. H. Chen, Y. He, G.J. Shiflet, and S.J. Poon: *Scripta Metall.*, 1991, vol. 25, pp. 1421–24.
12. F. Szuecs, C.P. Kim, and W.L. Johnson: *Acta Mater.*, 2001, vol. 49, pp. 1507–13.

13. M.C. Gao and G.J. Shiflet: *Scripta Mater.*, 2005, vol. 53, pp. 1129–34.
14. R.E. Hackenberg, M.C. Gao, L. Kaufman, and G.J. Shiflet: *Acta Mater.*, 2002, vol. 50, pp. 2245–58.
15. T.B. Massalski, H. Okamoto, P.R. Subramanian, and L. Kacprzak: *Binary Alloy Phase Diagrams*, ASM INTERNATIONAL, Materials Park, OH, 1990.
16. H. Okamoto: *Desk Handbook Phase Diagrams for Binary Alloys*, ASM INTERNATIONAL, Materials Park, OH, 2000.
17. M.C. Gao, N. Unlu, G.J. Shiflet, M. Mihalkovic, and M. Widom: *Metall. Mater. Trans. A*, 2005, vol. 36A, pp. 3269–79.
18. R.O. Jones and O. Gunnarsson: *Rev. Mod. Phys.*, 1989, vol. 61, pp. 689–746.
19. A.N. Mansour, C.P. Wong, and R.A. Brizzolara: *Phys. Rev. B*, 1994, vol. 50, pp. 12401–12.
20. P. Villars, A. Prince, and H. Okamoto: *Handbook of Ternary Alloy Phase Diagrams*, ASM INTERNATIONAL, Materials Park, OH, 1995.
21. O.S. Zarechnyuk, Z.M. Rykhal, and V.V. Korin: *Dopo. Akad. Nauk Ukr. A Fiziko.-Mater. Tekh Nauki*, 1980, vol. 42, pp. 84–85.
22. G. Kresse and J. Hafner: *Phys. Rev. B*, 1993, vol. 47, pp. 558–61.
23. G. Kresse and J. Furthmueller: *Phys. Rev. B*, 1996, vol. 54, pp. 11169–86.
24. G. Kresse and D. Joubert: *Phys. Rev. B*, 1999, vol. 59, pp. 1758–75.
25. M.C. Gao, A.D. Rollett, and M. Widom: *CALPHAD*, 2006, vol. 30, pp. 341–48.
26. J.P. Perdew, K. Burke, and M. Ernzerhof: *Phys. Rev. Lett.*, 1996, vol. 77, pp. 3865–8.
27. http://alloy.phys.cmu.edu (special "published" entries).
28. M. Mihalkovič and M. Widom: *Phys. Rev. B*, 2007, vol. 75, p. 014207.
29. M. Mihalkovic and M. Widom: *Phys. Rev. B*, 2004, vol. 70, p. 144107.
30. X.L. Ma and K.H. Kuo: *Metall. Mater. Trans. A*, 1994, vol. 25A, pp. 47–56.
31. T. Godecke and M. Ellner: *Z. Metallkd.*, 1996, vol. 87, pp. 854–64.
32. B. Grushko, R. Wittenberg, K. Bickman, and C. Freiburg: *J. Alloys Compd.*, 1996, vol. 233, pp. 279–87.
33. T. Godecke: *Z. Metallkd.*, 1997, vol. 88, pp. 904–10.
34. B. Grushko, C. Freiburg, K. Bickmann, and R. Wittenberg: *Z. Metallkd.*, 1997, vol. 88, pp. 379–81.
35. M. Mihalkovič and M. Widom: *MRS Symp. Proc.*, 2004, vol. 805, p. LL2.3.
36. M.C. Gao, G.J. Shiflet, M. Mihalkovic, and M. Widom: University of Virginia, unpublished research, 2002–2004.
37. E. Cockayne and M. Widom: *Phys. Rev. Lett.*, 1998, vol. 81, pp. 598–601.
38. M. Hillert and L.I. Staffanson: *Acta Chem. Scand.*, 1970, vol. 24, pp. 3618–26.
39. A.T. Dinsdale: *CALPHAD*, 1991, vol. 15, pp. 317–425.
40. O. Redlich and A.T. Kister: *Ind. Eng. Chem.*, 1948, vol. 40, pp. 345–8.
41. Y.M. Muggianu, M. Gambino, and J.P. Bros: *J. Chim. Phys.*, 1975, vol. 22, pp. 83–88.
42. N. Dupin and I. Ansara: *Rev. Metall.-Cahiers D Info. Technol.*, 1998, vol. 95, pp. 1121–9.
43. X.P. Su, W.J. Zhang, and Z.M. Du: *J. Alloys Compd.*, 1998, vol. 267, pp. 121–7.
44. C.H. Wu, Y.C. Chuang, and X.M. Jin: *J. Alloys Compd.*, 1992, vol. 179, pp. 27–35.
45. H.H. Stadelmaier, B. Reinsch, and G. Petzow: *Z. Metallkd.*, 1998, vol. 89, pp. 114–8.
46. G. Cacciamani and R. Ferro: *CALPHAD*, 2001, vol. 25, pp. 583–97.
47. O.S. Zarechnyuk and P.I. Kripyakevich: *Sov. Phys.-Cryst.*, 1962, vol. 7, p. 436.
48. G. Cordier, G. Dorsam, and R. Kniep: *J. Magn. Magn. Mater.*, 1988, vol. 76, pp. 653–4.
49. R.C. Mansey, G.V. Raynor, and I.R. Harris: *J. Less-Common Met.*, 1968, vol. 14, pp. 337–47.
50. N. Grin Yu, O.M. Sichevich, V.A. Bruskov, R.M. Rykhal, and P. Yarmolyuk Ya: *Sov. Phys.-Cryst.*, 1983, vol. 28, p. 346.
51. B. Sundman, B. Jansson, and J.O. Andersson: *CALPHAD*, 1985, vol. 9, pp. 153–90.
52. M. Asta, R. McCormack, and D. de Fontaine: *Phys. Rev. B*, 1993, vol. 48, pp. 748–66.
53. V. Ozolins, C. Wolverton, and A. Zunger: *Phys. Rev. B*, 1998, vol. 57, pp. 6427–43.
54. M. Asta and V. Ozolins: *Phys. Rev. B*, 2001, vol. 64, p. 094104 .
55. C. Wolverton: *Acta Mater.*, 2001, vol. 49, pp. 3129–42.
56. C. Wolverton, X.Y. Yan, R. Vijayaraghavan, and V. Ozolins: *Acta Mater.*, 2002, vol. 50, pp. 2187–97.
57. Y. Wang, S. Curtarolo, C. Jiang, R. Arroyave, T. Wang, G. Ceder, L.Q. Chen, and Z.K. Liu: *CALPHAD*, 2004, vol. 28, pp. 79–90.
58. Y. Zhong, C. Wolverton, Y.A. Chang, and Z.K. Liu: *Acta Mater.*, 2004, vol. 52, pp. 2739–54.
59. G. Ghosh and M. Asta: *Acta Mater.*, 2005, vol. 53, pp. 3225–52.
60. K. Ozturk, Y. Zhong, L.Q. Chen, C. Wolverton, J.O. Sofo, and Z.K. Liu: *Metall. Mater. Trans. A*, 2005, vol. 36A, pp. 5–13.
61. P.E.A. Turchi, V. Drchal, J. Kudrnovsky, C. Colinet, L. Kaufman, and Z.K. Liu: *Phys. Rev. B*, 2005, vol. 71, p. 094206.
62. P. Villars: *Pearson's Handbook,Desk ed.*, ASM INTERNATIONAL, Metals Park, OH, 1995.